

# Topology and edge modes surviving criticality in non-Hermitian Floquet systems

Longwen Zhou<sup>1, 2, 3, \*</sup>

<sup>1</sup>College of Physics and Optoelectronic Engineering,  
Ocean University of China, Qingdao, China 266100

<sup>2</sup>Key Laboratory of Optics and Optoelectronics, Qingdao, China 266100

<sup>3</sup>Engineering Research Center of Advanced Marine Physical Instruments and Equipment of MOE, Qingdao, China 266100

(Dated: 2026-02-16)

The discovery of critical points that can host quantized nonlocal order parameters and degenerate edge modes relocate the study of symmetry-protected topological phases (SPTs) to gapless regions. In this letter, we reveal gapless SPTs (gSPTs) in systems tuned out-of-equilibrium by periodic drivings and non-Hermitian couplings. Focusing on one-dimensional models with sublattice symmetry, we introduce winding numbers by applying the Cauchy's argument principle to generalized Brillouin zone (GBZ), yielding unified topological characterizations and bulk-edge correspondence in both gapped phases and at gapless critical points. The theory is demonstrated in a broad class of Floquet bipartite lattices, unveiling unique topological criticality of non-Hermitian Floquet origin. Our findings identify gSPTs in driven open systems and uncover robust topological edge modes at phase transitions beyond equilibrium.

*Introduction.*—Featured by coexistent bulk fluctuations and symmetry-protected edge modes, gSPTs blend the physics of quantum criticality and topology into a single context [1]. The survival of topological edge modes at critical points further allows the storage of localized information across phase transitions [2], whose stability could be of great use in quantum technologies. Following theoretical progress [3–38], observations of gSPTs were made in superconducting processors and acoustic waveguides [39–41], attracting continued interest over the years.

Floquet drivings and non-Hermitian effects are two means to impel a system out of equilibrium. The former could induce symmetry-breaking and topological transitions [42–44], create long-range-coupled phases with large topological numbers [45–47], and generate anomalous edge modes without static counterparts [48–50]. The latter could enrich the symmetry classification of topological matter [51–53], yield exceptional points with enhanced sensitive [54–56], and lead to non-Hermitian skin effects (NHSEs) that challenging the Bloch-band theory [57–59]. Their cooperation further results in non-Hermitian Floquet phases with unique topology [60], whose characterizations were yet mostly focused on gapped cases.

This letter establishes a framework to depict the gapless bulk topology,  $0/\pi$  edge modes and bulk-edge correspondence at non-Hermitian Floquet criticality. Our approach extends a recent theory of Floquet quantum criticality [61–63] by incorporating the GBZ scheme [64–66], making it applicable to the gaplessness of both Bloch and non-Bloch Floquet bands [67–69]. The theory is demonstrated in a set of Floquet non-Hermitian Su-Schrieffer-Heeger (NHSSH) chains and developed more systematically in the Supplementary Material (SM). A unified view is offered by investigating the phase diagram, edge states, phase transitions along topological phase boundaries and

scaling of entanglement entropy (EE). Notably, we identify nontrivial critical points and critical edge modes originated essentially from non-Hermitian Floquet drivings.

*Theory.*—We start by noting that any (non-)Hermitian Bloch Hamiltonian of a one-dimensional (1D), two band system with sublattice symmetry can be formally expressed as  $H(k) = f(k)\sigma_+ + g(k)\sigma_-$ , where  $\sigma_{\pm} \equiv (\sigma_x \pm i\sigma_y)/2$ ,  $\sigma_{x,y,z}$  are Pauli matrices, and the sublattice symmetry  $\Gamma = \sigma_z$  acts on  $H(k)$  as  $\Gamma H(k)\Gamma = -H(k)$ . The  $2\pi$ -periodicity of  $H(k)$  in quasimomentum  $k$  allows one to expand  $f(k)$  and  $g(k)$  as polynomials of  $e^{ik}$ . Continuing  $e^{ik} \rightarrow z$  to the whole complex plane and tracing the zero/pole locations of polynomial  $f(z)/g(z)$  yield a topological invariant  $w$ , which could classify all gapped phases of  $H(z)$  and predict a bulk-edge correspondence consisting with the non-Bloch band theory [70–72]. However, this approach is not directly applicable at the gap-closing point of  $H(z)$  [73], not to mention the Floquet case. The underlying reason is at least twofold. First, the non-Hermiticity of  $H(z)$  implies  $f(z) \neq g^*(z)$ , so that the criticality in  $f(z)$  and  $g(z)$  must be treated simultaneously at phase transitions instead of being depicted by a single ratio. Second, the spectrum of a Floquet operator could be gapless at both  $0$  and  $\pi$  quasienergies [74–76]. Such a “gap-doubling” is of temporal origin, making it impossible to capture its associated topology and phase transitions by a single static Hamiltonian.

To proceed, we express the Floquet operator  $U(k) = \hat{\mathcal{T}} e^{-\frac{i}{\hbar} \int_{t'}^{t'+T} H(k,t) dt}$  of the system in symmetric time frames [74] by selecting the initial time of evolution  $t'$ , so that the symmetrized Floquet operator  $U_s(k)$  unfolds the sublattice symmetry as  $\Gamma U_s(k)\Gamma = U_s^{-1}(k)$  ( $s = 1, 2$ ). Here, the Hamiltonian  $H(k, t) = H(k, t + T)$  has the driving period  $T$ , and  $\hat{\mathcal{T}}$  performs time ordering. In time frame  $s$ , the effective Hamiltonian of  $U_s(k)$  reads  $[U_s^{-1}(k) - U_s(k)]/(2i)$ , which must have the form  $H_s(k) = p_s(k)\sigma_+ + q_s(k)\sigma_-$  due to its sublattice symmetry. Taking the continuation  $k \rightarrow -i \ln z$ , we find a char-

\* zhoulw13@u.nus.edu

acteristic function of  $H_s(z)$  as  $f_s(z) = p_s(z)$  ( $= q_s(z)$ ) if  $m > m'$  ( $m' > m$ ), where  $m$  and  $m'$  are the highest positive powers of  $p_s(z)$  and  $q_s(z)$  in  $z$ . Finding the numbers of zeros  $N_s^z$  and poles  $N_s^p$  of  $f_s(z)$  inside the GBZ of  $H_s(z)$  then yields a winding number  $w_s$  following Cauchy's argument principle, i.e.,

$$w_s \equiv \begin{cases} N_s^z - N_s^p, & \Delta_\pi \neq 0 \\ N_s^z - N_s^p/2, & \Delta_\pi = 0 \end{cases}, \quad (1)$$

where  $\Delta_\pi \equiv \min_{z \in \text{GBZ}} |E(z) - \pi|$  infers whether  $U_s(z)$  has a gap at quasienergy  $E = \pi$  along the Floquet GBZ (FGBZ). Combining the  $(w_1, w_2)$  defined in two time frames yields the topological invariants

$$(w_0, w_\pi) = \frac{1}{2}(w_1 + w_2, w_1 - w_2) \in \mathbb{Z} \times \mathbb{Z}. \quad (2)$$

They offer a unified characterization for all gapped and gapless non-Hermitian Floquet phases in 1D, two-band, sublattice-symmetric systems. The numbers of edge modes at 0 and  $\pi$  quasienergies are related to these invariants according to the bulk-edge correspondence

$$(N_0, N_\pi) = 2(|w_0|, |w_\pi|). \quad (3)$$

We emphasize that Eqs. (1)–(3) are generic, in the sense that they do not concern whether there exists a (point or line) gap in the spectrum and whether the underlying band theory is in Bloch or non-Bloch forms. The only relevant factors are spatial dimensions, number of bands and symmetries of the system. In Hermitian limits, where FGBZ reduces to the usual Brillouin zone, we end with the approach in Ref. [61]. Figs. 1(a)–(c) illustrate our theory applied to a case with gapless spectrum (see Sec. I of the SM for more details). Below, we work out an example to show the unique topology and edge modes at criticality in non-Hermitian Floquet systems.

*Model.*—We focus on a class of periodically quenched NHSSH (PQNHSSSH) models, which may be viewed as a stacking of SSH chains with two distinct hopping ranges in time domain. A sketch of the model is given in Fig. 1(d), where the Floquet operator reads  $\hat{U} = e^{-i\hat{\mathcal{H}}_\alpha} e^{-i\hat{\mathcal{H}}_{\alpha'}}$ ,  $\hat{\mathcal{H}}_\iota \equiv \sum_n (J_\iota^L \hat{b}_n^\dagger \hat{a}_{n+\iota} + J_\iota^R \hat{a}_n^\dagger \hat{b}_{n+\iota})$ , the hopping amplitude  $J_\iota^{\text{L},\text{R}} \equiv t_\iota^{\text{L},\text{R}} T/(2\hbar)$  for  $\iota = \alpha, \alpha'$ , and  $\hat{a}_n^\dagger$  ( $\hat{b}_n^\dagger$ ) creates a particle in sublattice A (B) of unit cell  $n$ . To evaluate the winding numbers, we need to transform  $\hat{U}$  to symmetric time frames. Taking the initial time of evolution as  $t' = T/4$  and  $3T/4$  yield Floquet operators

$$\hat{\mathcal{U}}_{1(2)} = e^{-\frac{i}{2}\hat{\mathcal{H}}_{\alpha'(\alpha)}} e^{-i\hat{\mathcal{H}}_{\alpha(\alpha')}} e^{-\frac{i}{2}\hat{\mathcal{H}}_{\alpha'(\alpha)}}, \quad (4)$$

where the sublattice symmetry  $\hat{\Gamma} = \sum_n (\hat{a}_n^\dagger \hat{a}_n - \hat{b}_n^\dagger \hat{b}_n)$  is retained as  $\hat{\Gamma} \hat{\mathcal{U}}_s \hat{\Gamma} = \hat{\mathcal{U}}_s^{-1}$  for  $s = 1, 2$ . This symmetry enforces the eigenstates of  $\hat{U}$  to come in pairs of opposite quasienergies  $\pm E$ . The Floquet bands of  $\hat{U}$  could thus meet at either  $E = 0$  or  $\pi$ , yielding phase transitions (criticality), with the latter being of Floquet origin. Be-

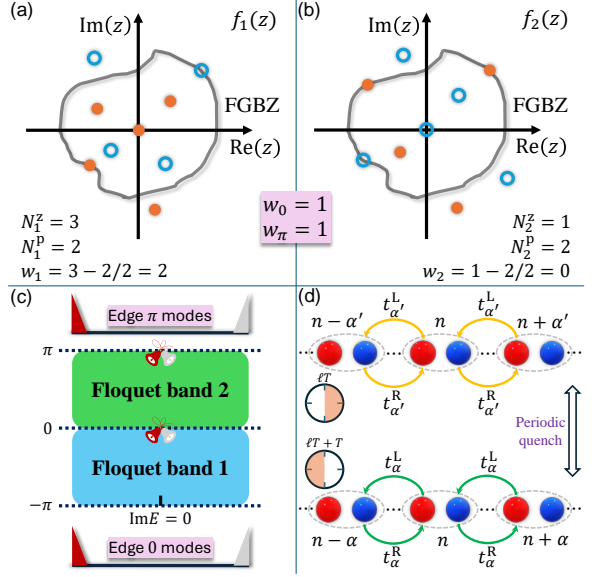


FIG. 1. Schematics of theory and model. (a) and (b) show the zero/pole locations of  $f_1(z)$  and  $f_2(z)$  on complex plane, with the wiggled contour showing the FGBZ. Orange dots (cyan circles) denote the zeros (poles) of  $f_{1,2}(z)$ . The spectrum related to (a), (b) is sketched in (c). The two bands are touched at both  $E = 0, \pi$ . The critical 0 ( $\pi$ ) edge modes are depicted by the bells hung at  $E = 0 (\pi)$ , with their profiles illustrated at the bottom (top) of (c). (d) shows the NHSSH model under periodic quenches. The red (blue) balls at the center of each chain denote sublattice A (B) of unit cell  $n$ .

low, we take  $0 \leq \alpha < \alpha'$  and let  $J_\alpha^{\text{L}} = J_\alpha^{\text{R}} = J_\alpha \in \mathbb{R}$  without losing the essence. Non-Hermitian effects then all come from nonreciprocal couplings  $J_{\alpha'}^{\text{L}} \neq (J_{\alpha'}^{\text{R}})^*$ . The model we introduced here will be called the PQNHSSH  $\alpha$ -chain (see Sec. II of the SM for details).

*Topology and bulk-edge correspondence.*—Under periodic boundary condition, the Floquet operators in Eq. (4) can be expressed in momentum space, and the FGBZ is obtained as (see Sec. II of the SM for derivations)

$$\beta = (J_{\alpha'}^{\text{R}}/J_{\alpha'}^{\text{L}})^{1/(2\alpha' - 2\alpha)} e^{i\theta}, \quad \theta \in [-\pi, \pi], \quad (5)$$

which is a circle of radius  $r = |\beta|$ . It deviates from the unit circle once  $|J_{\alpha'}^{\text{L}}| \neq |J_{\alpha'}^{\text{R}}|$ , yielding physics unique to non-Hermitian systems. The gap closing condition along FGBZ generates phase boundaries. Working it out explicitly with  $(J_{\alpha'}^{\text{L}}, J_{\alpha'}^{\text{R}}) \equiv (J - \gamma, J + \gamma)$ , we find the critical lines  $J_\alpha \pm \sqrt{J^2 - \gamma^2} = \nu\pi$  for  $|\gamma| \leq |J|$  and  $\cos(J_\alpha) \cosh(\sqrt{\gamma^2 - J^2}) = (-1)^\nu$  for  $|\gamma| > |J|$  ( $\nu \in \mathbb{Z}$ ). They yield the red curves in Fig. 2. They are distinct from those found in Hermitian [61] or non-driven [73] limits, and can be topologically allocated into four groups.

To unveil the bulk topology, we compute the  $(w_0, w_\pi)$  in Eq. (2) analytically and report them for each phase in Fig. 2 (see Sec. II of the SM for details). Although the gapped phases with  $(w_0, w_\pi) = (\alpha, 0)$  and  $(\alpha', 0)$  are realizable in equilibrium [73], the phases with  $w_\pi = \alpha' - \alpha$

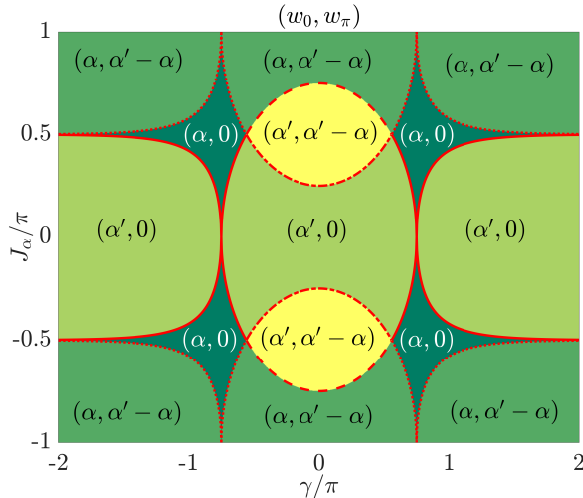


FIG. 2. Phase diagram of PQNHSSH  $\alpha$ -chain. Hopping amplitudes over  $\alpha'$  unit cells are  $J_{\alpha'}^{\text{L(R)}} = J - (+)\gamma$ . Regions of distinct colors are gapped phases, with their topological indices  $(w_0, w_\pi)$  shown explicitly. Red solid (dotted) lines have  $(w_0, w_\pi) = (\alpha, 0)$ , with bulk gap closes at  $E = 0$  ( $\pi$ ). Red dash-dotted lines have  $(w_0, w_\pi) = (\alpha', 0)$ , with bulk gap closes at  $E = \pi$ . Red dashed lines have  $(w_0, w_\pi) = (\alpha, \alpha' - \alpha)$ , with bulk gap closes at  $E = 0$ .

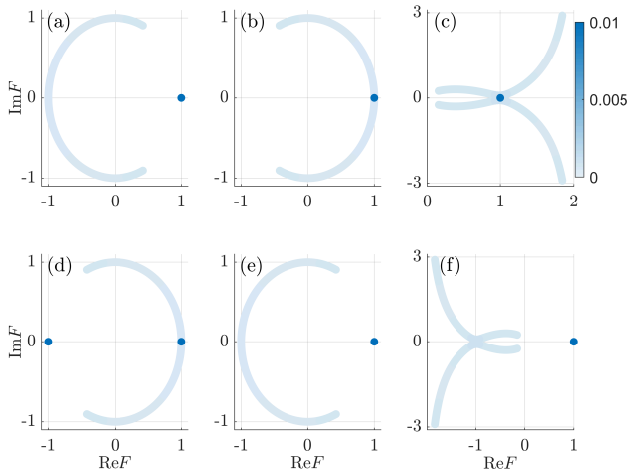


FIG. 3. Spectra of PQNHSSH  $\alpha$ -chain at criticality with  $(\alpha, \alpha') = (1, 2)$ , shown in terms of the Floquet operator's eigenvalue  $F \equiv e^{-iE}$ . The color of each point records the inverse participation ratio (IPR) of related state in a lattice with 1000 unit cells. System parameters are  $J_1^{\text{L}} = J_1^{\text{R}} = J_1$ ,  $(J_2^{\text{L}}, J_2^{\text{R}}) = (J - \gamma, J + \gamma)$ ,  $J = 3\pi/4$  for all panels, and  $J_1 = 0.32\pi$  ( $0.68\pi$ ) for (a)-(c) ((d)-(f)).  $\gamma = \sqrt{J^2 - (\pi - J_1)^2}$  for (a,e),  $\sqrt{J^2 - J_1^2}$  for (b,d),  $\sqrt{J^2 + \text{acosh}^2(1/\cos J_1)}$  for (c) and  $\sqrt{J^2 + \text{acosh}^2(-1/\cos J_1)}$  for (f).

are unique to non-Hermitian Floquet setups, with each of them having  $2(\alpha' - \alpha)$  topological edge modes at  $E = \pi$  [Eq. (3)]. The topology of these anomalous Floquet phases are thus captured by our theory, even though they both subject to NHSEs and the violation of standard

bulk-edge correspondence if  $\gamma \neq 0$ .

Strikingly, the invariants in Eq. (2) are also well-defined and quantized at phase transitions. Along the red solid critical lines where  $|\tan(\sqrt{J^2 - \gamma^2}/2)| = |\tan(J_\alpha/2)|$  in Fig. 2, the gap closes at  $E = 0$  and  $(w_0, w_\pi) = (\alpha, 0)$ . They are thus topologically nontrivial, having  $N_0 = 2\alpha$  edge 0 modes with a gapless bulk at  $E = 0$  for  $\alpha > 0$ . Along the red dash-dotted critical lines where  $|\tan(\sqrt{J^2 - \gamma^2}/2) \tan(J_\alpha/2)| = 1$  in Fig. 2, the gap closes at  $E = \pi$  and  $(w_0, w_\pi) = (\alpha', 0)$ . They are always topologically nontrivial, having  $N_0 = 2\alpha'$  edge 0 modes with a gapless bulk at  $E = \pi$ . The red dotted critical lines in Fig. 2 also satisfy  $|\tan(\sqrt{J^2 - \gamma^2}/2) \tan(J_\alpha/2)| = 1$ , where the gap closes at  $E = \pi$  and  $(w_0, w_\pi) = (\alpha, 0)$ . They are topologically nontrivial, with  $2\alpha$  edge 0 modes coexisting with a gapless bulk at  $E = \pi$  if  $\alpha > 0$ . Notably, these two groups of transitions are absent when the driving is switched off [73], which implies their Floquet origins. Finally, the red dashed critical lines in Fig. 2 satisfy  $|\tan(\sqrt{J^2 - \gamma^2}/2)| = |\tan(J_\alpha/2)|$  with the gap closing at  $E = 0$  and  $(w_0, w_\pi) = (\alpha, \alpha' - \alpha)$ . They are topologically nontrivial with  $2\alpha$  and  $2(\alpha' - \alpha)$  edge modes at  $E = 0$  and  $\pi$ . Non-Hermitian Floquet gSPTs reveal along these critical lines for any  $0 \leq \alpha < \alpha'$ . A summary of the topology and edge modes at four distinct phase boundaries in Fig. 2 is given in Table I of the End Matter. It deserves to mention that all critical lines in Fig. 2 refer to gap-closings between Floquet non-Bloch bands over FGBZ. A naive application of Bloch band theory cannot yield consistent phase boundaries and bulk-edge correspondence at criticality.

*Critical edge modes.*—To further reveal edge modes associated with non-Hermitian Floquet topology at phase transitions, we obtain the quasienergies under open boundary condition (OBC) with  $(\alpha, \alpha') = (1, 2)$ . The spectra in Figs. 3(a), (b), (d) and (e) are obtained at exemplary points along the dashed-dotted, solid, dashed and dotted critical lines of Fig. 2 in its  $\mathcal{PT}$ -unbroken region ( $|\gamma| < |J|$ ). The probability distributions of their edge modes are shown in (a), (b), (c) and (d) of Fig. 6 in the End Matter, with the bands touching at  $E = \pi$  ( $F = -1$ ),  $0$  ( $F = 1$ ),  $0$  and  $\pi$ . Our bulk theory [Eq. (3)] predicts the numbers of edge modes  $(N_0, N_\pi) = (4, 0)$ ,  $(2, 0)$ ,  $(2, 2)$  and  $(2, 0)$  at these critical points, which are in perfect agreement with those observed in Fig. 6, verifying the bulk-edge correspondence at phase transitions. In the  $\mathcal{PT}$ -broken region ( $|\gamma| > |J|$ ), the range of exponential  $e^{-iE}$  goes beyond the unit circle  $|F| = 1$ , as shown in Figs. 3(c) and 3(f). Nevertheless, we find two edge 0 modes at both these critical points, regardless of whether the bulk gap closes at  $E = 0$  [ $F = 1$  in Fig. 3(c)] or  $E = \pi$  [ $F = -1$  in Fig. 3(f)], and their distributions are identical to those in (b) and (d) of Fig. 6. Lying along the solid and dotted lines in Fig. 2, the numbers of edge modes at these critical points are  $(N_0, N_\pi) = (2, 0)$ , verifying again the Eq. (3). Overall, we confirmed the nontrivial topology and edge modes surviving critical-

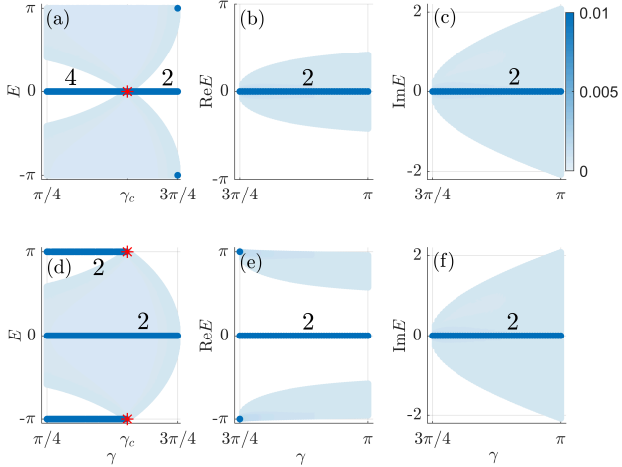


FIG. 4. Floquet spectra along critical lines. The color of each point records the IPR of related state in a lattice with 1000 unit cells. Numbers of 0 and  $\pi$  edge modes are given in each panel. In (a) ((d)), parameters are varied along the dash-dotted to dotted (dashed to solid) lines in Fig. 2 for  $\gamma = \pi/4 \rightarrow 3\pi/4$ . In (b)–(c) ((e)–(f)), parameters are varied along the dotted (solid) line in Fig. 2 for  $\gamma = 3\pi/4 \rightarrow \pi$ .

ity in our setting, regardless of whether the underlying quasienergy spectrum is in  $\mathcal{PT}$ -invariant or  $\mathcal{PT}$ -broken regime. In the End Matter, we give exact solutions of topological edge modes at non-Hermitian Floquet criticality (see Sec. II of the SM for derivations), which offer analytical justifications for our theory.

*Phase transitions between gSPTs.*—With four critical lines of different topology, we expect to see phase transitions along topological phase boundaries via changing system parameters across the multicritical point. In Fig. 4, we present the spectrum of our model with  $(\alpha, \alpha') = (1, 2)$  along phase boundaries, where the star denotes the multicritical point  $(J_1, \gamma_c) = (\pi/2, \sqrt{5}\pi/4)$ . In (a) and (d) of Fig. 4, we find a change of 0 and  $\pi$  edge modes by 2 when going from one to the other side of multicritical point, during which the spectrum remains gapless at  $E = \pi$  and 0, respectively. The  $(w_0, w_\pi)$  in Eq. (2) change from  $(2, 0)$  [ $(1, 1)$ ] to  $(1, 0)$  across the multicritical point in Fig. 4(a) [4(d)]. These cases represent two examples of phase transitions between distinct non-Hermitian Floquet gSPTs, which are identified by the survival of edge zero modes at criticality. In Figs. 4(b,c) and 4(e,f), we show the spectra along two critical lines in the  $\mathcal{PT}$ -broken region, with bulk bands touched at  $E = 0$  and  $\pi$ . There are no multicritical points on these phase boundaries, and we find two edge 0 modes in both cases, even though gain and loss are existent in the critical bulk. In all cases, the degeneracy of 0 and  $\pi$  edge modes are protected by the sublattice symmetry.

The necessity of discriminating phase transitions via topology can also be seen from entanglement viewpoints. In Fig. 5, we extract the central charge of bipartite EE at half-filling in a  $\mathcal{PT}$ -unbroken region ( $|\gamma| < |J|, J_\alpha > 0$ )

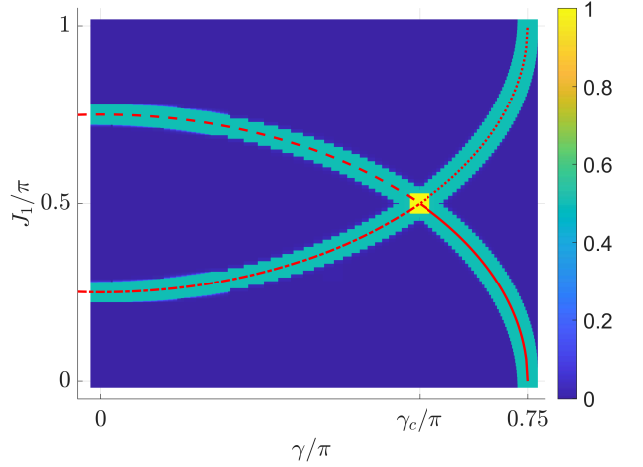


FIG. 5. Central charge of PQNHSSH  $\alpha$ -chain with  $(\alpha, \alpha') = (1, 2)$ . System parameters are  $(J_2^L, J_2^R) = (J - \gamma, J + \gamma)$  with  $J = 3\pi/4$ . The fitting curve  $S(L, l) \sim 2c \ln[\sin(\pi l/L)]/3$  is used for bipartite EE at half-filling with total system size  $L = 1000$  and varied subsystem sizes  $l$ .

of Fig. 2. Despite the multicritical point where  $c = 1$ , we find  $c = 1/2$  along critical lines. The former comes about due to the simultaneous gap closing of Floquet non-Bloch bands at  $E = 0$  and  $\pi$ , which is thus of nonequilibrium origin. The latter implies that the critical lines in Fig. 5 may belong to the same universality class, which can only be distinguished by their topology and edge modes. For other hopping ranges  $(\alpha, \alpha')$ , we expect  $c = (\alpha' - \alpha)/2$  along critical lines (with  $J_1 \rightarrow J_\alpha$  in Fig. 5) and  $c = \alpha' - \alpha$  at multicritical points (see Sec. III of the SM for details).

*Discussion.*—Experimentally, the Hermitian version of our model is realizable in acoustics [41], where the quasienergies are accessible by a pump-probe method, and the driving is emulated by modulations along the propagation direction of sound. By recording both the amplitude and phase of pressure fields, the Floquet bands can be constructed from phase-resolved measurements, allowing the identification of whether the system is away from or at a gapless phase transition [41]. The critical 0 and  $\pi$  modes can be further detected by tracking the dynamics of edge excitations [77]. Finally, the non-Hermiticity, as introduced by asymmetric couplings in our case, can be realized with directional amplifiers in acoustic crystals [78]. Acoustic metamaterials thus offer a flexible means to realize our model and detect its topology and edge modes surviving criticality. Other setups where our model is within reach include photonics [79–81] and electrical circuits [82–84]. In future work, it would be interesting to generalize our scheme to systems with multiple bands [85–87], in other symmetry classes [88], and beyond 1D cases [89]. Exceptional topology [90] of non-Hermitian Floquet origin and its impact on critical edge modes are awaited to be further clarified. The roles of disorder and interactions in non-Hermitian Floquet gSPTs also deserve more thorough explorations.

*Acknowledgments.*—L.Z. is supported by the NSFC (Grants No. 12275260 and No. 11905211), the Fundamen-

tal Research Funds for the Central Universities (Grant No. 202364008), and the Young Talents Project of Ocean University of China.

---

[1] T. Scaffidi, D. E. Parker, and R. Vasseur, Gapless Symmetry-Protected Topological Order, *Phys. Rev. X* **7**, 041048 (2017).

[2] R. Verresen, R. Thorngren, N. G. Jones, and F. Pollmann, Gapless Topological Phases and Symmetry-Enriched Quantum Criticality, *Phys. Rev. X* **11**, 041059 (2021).

[3] Y. Baum, T. Posske, I. C. Fulga, B. Trauzettel, and A. Stern, Coexisting Edge States and Gapless Bulk in Topological States of Matter, *Phys. Rev. Lett.* **114**, 136801 (2015).

[4] A. Keselman and E. Berg, Gapless symmetry-protected topological phase of fermions in one dimension, *Phys. Rev. B* **91**, 235309 (2015).

[5] S. C. Furuya and M. Oshikawa, Symmetry protection of critical phases and a global anomaly in 1+1 dimensions, *Phys. Rev. Lett.* **118**, 021601 (2017).

[6] R. Verresen, R. Moessner, and F. Pollmann, One-dimensional symmetry protected topological phases and their transitions, *Phys. Rev. B* **96**, 165124 (2017).

[7] R. Verresen, N. G. Jones, and F. Pollmann, Topology and Edge Modes in Quantum Critical Chains, *Phys. Rev. Lett.* **120**, 057001 (2018).

[8] W. Berdanier, M. Kolodrubetz, S. A. Parameswaran, and R. Vasseur, Floquet quantum criticality, *Proc. Natl. Acad. Sci. U.S.A.* **115**, 9491-9496 (2018).

[9] N. G. Jones and R. Verresen, Asymptotic Correlations in Gapped and Critical Topological Phases of 1D Quantum Systems, *J. Stat. Phys.* **175**, 1164-1213 (2019).

[10] D. E. Parker, R. Vasseur and T. Scaffidi, Topologically protected long edge coherence times in symmetry-broken phases, *Phys. Rev. Lett.* **122**, 240605 (2019).

[11] R. Verresen, Topology and edge states survive quantum criticality between topological insulators, *arXiv:2003.05453*.

[12] O. Balabanov, D. Erkensten, and H. Johannesson, Topology of critical chiral phases: Multiband insulators and superconductors, *Phys. Rev. Res.* **3**, 043048 (2021).

[13] R. Thorngren, A. Vishwanath and R. Verresen, Intrinsically gapless topological phases, *Phys. Rev. B* **104**, 075132 (2021).

[14] C. M. Duque, H.-Y. Hu, Y.-Z. You, V. Khemani, R. Verresen, and R. Vasseur, Topological and symmetry-enriched random quantum critical points, *Phys. Rev. B* **103**, L100207 (2021).

[15] U. Borla, R. Verresen, J. Shah and S. Moroz, Gauging the Kitaev chain, *SciPost Phys.* **10**, 148 (2021).

[16] R. R. Kumar, Y. R. Kartik, S. Rahul, and S. Sarkar, Multi-critical topological transition at quantum criticality, *Sci. Rep.* **11**, 1004 (2021).

[17] X.-J. Yu, R.-Z. Huang, H.-H. Song, L. Xu, C. Ding and L. Zhang, Conformal boundary conditions of symmetry-enriched quantum critical spin chains, *Phys. Rev. Lett.* **129**, 210601 (2022).

[18] Y. Hidaka, S. C. Furuya, A. Ueda and Y. Tada, Gapless symmetry-protected topological phase of quantum anti-ferromagnets on anisotropic triangular strip, *Phys. Rev. B* **106**, 144436 (2022).

[19] R. Ma, L. Zou and C. Wang, Edge physics at the deconfined transition between a quantum spin Hall insulator and a superconductor, *SciPost Phys.* **12**, 196 (2022).

[20] N. G. Jones, R. Thorngren, and R. Verresen, Bulk-Boundary Correspondence and Singularity-Filling in Long-Range Free-Fermion Chains, *Phys. Rev. Lett.* **130**, 246601 (2023).

[21] R. Wen and A. C. Potter, Bulk-boundary correspondence for intrinsically gapless symmetry-protected topological phases from group cohomology, *Phys. Rev. B* **107**, 245127 (2023).

[22] H. Yang, L. Li, K. Okunishi and H. Katsura, Duality, criticality, anomaly, and topology in quantum spin-1 chains, *Phys. Rev. B* **107**, 125158 (2023).

[23] R. R. Kumar, N. Roy, Y. R. Kartik, S. Rahul, and S. Sarkar, Signatures of topological phase transition on a quantum critical line, *Phys. Rev. B* **107**, 205114 (2023).

[24] S. Mondal, A. Agarwala, T. Mishra, and A. Prakash, Symmetry-enriched criticality in a coupled spin ladder, *Phys. Rev. B* **108**, 245135 (2023).

[25] S. Prembabu, R. Thorngren, and R. Verresen, Boundary-deconfined quantum criticality at transitions between symmetry-protected topological chains, *Phys. Rev. B* **109**, L201112 (2024).

[26] L. Li, M. Oshikawa and Y. Zheng, Decorated defect construction of gapless-SPT states, *SciPost Phys.* **17**, 013 (2024).

[27] L. Li, M. Oshikawa and Y. Zheng, Intrinsically/purely gapless-SPT from non-invertible duality transformations, *SciPost Phys.* **18**, 153 (2025).

[28] R. Flores-Calderón, E. J. König, and A. M. Cook, Topological Quantum Criticality from Multiplicative Topological Phases, *Phys. Rev. Lett.* **134**, 116602 (2025).

[29] H. Jia, J. Hu, R.-Y. Zhang, Y. Xiao, D. Wang, M. Wang, S. Ma, X. Ouyang, Y. Zhu, and C. T. Chan, Unconventional Topological Edge States In One-Dimensional Non-Hermitian Gapless Systems Stemming from Nonisolated Hypersurface Singularities, *Phys. Rev. Lett.* **134**, 206603 (2025).

[30] C. Song, Zero Curvature Condition for Quantum Criticality, *Phys. Rev. Lett.* **134**, 240202 (2025).

[31] X. Shen, Z. Wu, and S.-K. Jian, Boundary and defect criticality in topological insulators and superconductors, *Phys. Rev. B* **112**, L041118 (2025).

[32] A. Chatterjee, W. Ji, and X.-G. Wen, Emergent generalized symmetry and maximal symmetry topological order, *Phys. Rev. B* **112**, 115142 (2025).

[33] G. Cardoso, H.-C. Yeh, L. Korneev, A. G. Abanov, and A. Mitra, Gapless Floquet topology, *Phys. Rev. B* **111**, 125162 (2025).

[34] R. Wen and A. C. Potter, Classification of 1+1D gapless symmetry protected phases via topological holography, *Phys. Rev. B* **111**, 115161 (2025).

[35] X. Zhou, S. Jia, and J.-S. Pan, Interaction-induced phase

transitions at topological quantum criticality of an extended Su-Schrieffer-Heeger model, *Phys. Rev. B* **111**, 195117 (2025).

[36] L. Li, R.-Z. Huang, and W. Cao, Noninvertible symmetry-enriched quantum critical point, *Phys. Rev. B* **112**, L081113 (2025).

[37] S.-J. Huang and M. Cheng, Topological holography, quantum criticality, and boundary states, *SciPost Phys.* **18**, 213 (2025).

[38] R. Barad, Q. Tang, W. Zhu, and X. Wen, Universal time evolution of string order parameter in quantum critical systems with boundary invertible or noninvertible symmetry breaking, *Phys. Rev. B* **111**, 165121 (2025).

[39] R. Shen, T. Chen, B. Yang, Y. Zhong, and C. H. Lee, Robust simulations of many-body symmetry-protected topological phase transitions on a quantum processor, *npj Quantum Inf.* **11**, 179 (2025).

[40] Z. Tan, K. Wang, S. Yang, et. al., Exploring nontrivial topology at quantum criticality in a superconducting processor, arXiv:2501.04679.

[41] Z. Cheng, X. Zhang, X.-J. Yu, L. Zhou, J. Gong, and B. Zhang, Observation of critical topological phase transition, *to appear*.

[42] T. Oka and H. Aoki, Photovoltaic Hall effect in graphene, *Phys. Rev. B* **79**, 081406(R) (2009).

[43] G. Jotzu, M. Messer, R. Desbuquois, M. Lebrat, T. Uehlinger, D. Greif, and T. Esslinger, Experimental realization of the topological Haldane model with ultracold fermions, *Nature* **515**, 237–240 (2014).

[44] J. W. McIver, B. Schulte, F.-U. Stein, T. Matsuyama, G. Jotzu, G. Meier, and A. Cavalleri, Light-induced anomalous Hall effect in graphene, *Nat. Phys.* **16**, 38–41 (2020).

[45] D. Y. H. Ho and J. Gong, Quantized Adiabatic Transport In Momentum Space, *Phys. Rev. Lett.* **109**, 010601 (2012).

[46] Q.-J. Tong, J.-H. An, J. Gong, H.-G. Luo, and C. H. Oh, Generating many Majorana modes via periodic driving: A superconductor model, *Phys. Rev. B* **87**, 201109(R) (2013).

[47] K. Yang, S. Xu, L. Zhou, Z. Zhao, T. Xie, Z. Ding, W. Ma, J. Gong, F. Shi, and J. Du, Observation of Floquet topological phases with large Chern numbers, *Phys. Rev. B* **106**, 184106 (2022).

[48] L. Jiang, T. Kitagawa, J. Alicea, A. R. Akhmerov, D. Pekker, G. Refael, J. I. Cirac, E. Demler, M. D. Lukin, and P. Zoller, Majorana Fermions in Equilibrium and in Driven Cold-Atom Quantum Wires, *Phys. Rev. Lett.* **106**, 220402 (2011).

[49] M. S. Rudner, N. H. Lindner, E. Berg, and M. Levin, Anomalous Edge States and the Bulk-Edge Correspondence for Periodically Driven Two-Dimensional Systems, *Phys. Rev. X* **3**, 031005 (2013).

[50] K. Wintersperger, C. Braun, F. N. Ünal, A. Eckardt, M. D. Liberto, N. Goldman, I. Bloch, and M. Aidelsburger, Realization of an anomalous Floquet topological system with ultracold atoms, *Nat. Phys.* **16**, 1058–1063 (2020).

[51] K. Kawabata, K. Shiozaki, M. Ueda, and M. Sato, Symmetry and Topology in Non-Hermitian Physics, *Phys. Rev. X* **9**, 041015 (2019).

[52] H. Zhou and J. Y. Lee, Periodic table for topological bands with non-Hermitian symmetries, *Phys. Rev. B* **99**, 235112 (2019).

[53] C. M. Bender and D. W. Hook,  $\mathcal{PT}$ -symmetric quantum mechanics, *Rev. Mod. Phys.* **96**, 045002 (2024).

[54] W. D. Heiss, The physics of exceptional points, *J. Phys. A: Math. Theor.* **45**, 444016 (2012).

[55] J. Wiersig, Enhancing the sensitivity of frequency and energy splitting detection by using exceptional points: Application to microcavity sensors for single-particle detection, *Phys. Rev. Lett.* **112**, 203901 (2014).

[56] M.-A. Miri and A. Alù, Exceptional points in optics and photonics, *Science* **363**, eaar7709 (2019).

[57] S. Yao and Z. Wang, Edge States and Topological Invariants of Non-Hermitian Systems, *Phys. Rev. Lett.* **121**, 086803 (2018).

[58] F. K. Kunst, E. Edvardsson, J. C. Budich, and E. J. Bergholtz, Biorthogonal Bulk-Boundary Correspondence in Non-Hermitian Systems, *Phys. Rev. Lett.* **121**, 026808 (2018).

[59] V. M. Martinez Alvarez, J. E. Barrios Vargas, and L. E. F. Foa Torres, Non-Hermitian robust edge states in one dimension: Anomalous localization and eigenspace condensation at exceptional points, *Phys. Rev. B* **97**, 121401(R) (2018).

[60] L. Zhou and D.-J. Zhang, Non-Hermitian Floquet Topological Matter—A Review, *Entropy* **25**, 1401 (2023).

[61] L. Zhou, J. Gong, and X.-J. Yu, Topological edge states at Floquet quantum criticality, *Commun. Phys.* **8**, 214 (2025).

[62] L. Zhou, R. Wang, and J. Pan, Gapless higher-order topology and corner states in Floquet systems, *Phys. Rev. Res.* **7**, 023079 (2025).

[63] L. Zhou, F. Zhang, and J. Pan, Floquet Möbius topological insulators, *Phys. Rev. B* **112**, 134302 (2025).

[64] K. Yokomizo and S. Murakami, Non-Bloch Band Theory of Non-Hermitian Systems, *Phys. Rev. Lett.* **123**, 066404 (2019).

[65] Z. Yang, K. Zhang, C. Fang, and J. Hu, Non-Hermitian Bulk-Boundary Correspondence and Auxiliary Generalized Brillouin Zone Theory, *Phys. Rev. Lett.* **125**, 226402 (2020).

[66] Y. Cao, Y. Li, and X. Yang, Non-Hermitian bulk-boundary correspondence in a periodically driven system, *Phys. Rev. B* **103**, 075126 (2021).

[67] L. Zhou and J. Gong, Non-Hermitian Floquet topological phases with arbitrarily many real-quasienergy edge states, *Phys. Rev. B* **98**, 205417 (2018).

[68] L. Xiao, T. Deng, K. Wang, G. Zhu, Z. Wang, W. Yi, and P. Xue, Non-Hermitian bulk-boundary correspondence in quantum dynamics, *Nat. Phys.* **16**, 761–766 (2020).

[69] X. Zhang and J. Gong, Non-Hermitian Floquet topological phases: Exceptional points, coalescent edge modes, and the skin effect, *Phys. Rev. B* **101**, 045415 (2020).

[70] C. H. Lee and R. Thomale, Anatomy of skin modes and topology in non-Hermitian systems, *Phys. Rev. B* **99**, 201103(R) (2019).

[71] S. Verma and M. J. Park, Topological phase transitions of generalized Brillouin zone, *Commun. Phys.* **7**, 21 (2024).

[72] J. Zhong, H. Wang, and S. Fan, Pole and zero edge state invariant for one-dimensional non-Hermitian sublattice symmetry, *Phys. Rev. B* **110**, 214113 (2024).

[73] L. Zhou, R. Jing, and S. Wu, Topological characterization of phase transitions and critical edge states in one-dimensional non-Hermitian systems with sublattice symmetry, *Front. Phys.* **21**, 075202 (2026).

[74] J. K. Asbóth and H. Obuse, Bulk-boundary correspondence for chiral symmetric quantum walks, *Phys. Rev. B* **88**, 121406(R) (2013).

- [75] M. Rodriguez-Vega and B. Seradjeh, Universal Fluctuations of Floquet Topological Invariants at Low Frequencies, *Phys. Rev. Lett.* **121**, 036402 (2018).
- [76] L. Zhou and J. Gong, Floquet topological phases in a spin-1/2 double kicked rotor, *Phys. Rev. A* **97**, 063603 (2018).
- [77] Z. Cheng, R. W. Bomantara, H. Xue, W. Zhu, J. Gong, and B. Zhang, Observation of  $\pi/2$  modes in an acoustic Floquet system, *Phys. Rev. Lett.* **129**, 254301 (2022).
- [78] L. Zhang, Y. Yang, Y. Ge, Y.-J. Guan, Q. Chen, Q. Yan, F. Chen, R. Xi, Y. Li, D. Jia, S.-Q. Yuan, H.-X. Sun, H. Chen, and B. Zhang, Acoustic non-Hermitian skin effect from twisted winding topology, *Nat. Commun.* **12**, 6297 (2021).
- [79] L. Xiao, T. Deng, K. Wang, Z. Wang, W. Yi, and P. Xue, Observation of Non-Bloch Parity-Time Symmetry and Exceptional Points, *Phys. Rev. Lett.* **126**, 230402 (2021).
- [80] J. Zhu, Y.-L. Mao, H. Chen, K.-X. Yang, L. Li, B. Yang, Z.-D. Li, and J. Fan, Observation of Non-Hermitian Edge Burst Effect in One-Dimensional Photonic Quantum Walk, *Phys. Rev. Lett.* **132**, 203801 (2024).
- [81] L. Xiao, W.-T. Xue, F. Song, Y.-M. Hu, W. Yi, Z. Wang, and P. Xue, Observation of Non-Hermitian Edge Burst in Quantum Dynamics, *Phys. Rev. Lett.* **133**, 070801 (2024).
- [82] T. Helbig, T. Hofmann, S. Imhof, M. Abdelghany, T. Kiessling, L. W. Molenkamp, C. H. Lee, A. Szameit, M. Greiter, and R. Thomale, Generalized bulk-boundary correspondence in non-Hermitian topoelectrical circuits, *Nat. Phys.* **16**, 747–750 (2020).
- [83] X. Zhou, W. Zhang, W. Cao, and X. Zhang, Non-Hermitian Floquet Topological Sensors for Ultrasensitive Detection of Dynamic Signals, *Phys. Rev. Lett.* **135**, 106601 (2025).
- [84] J. Zhang, W. Song, H. Li, Z. Kuang, Z. Xiong, L. Zhou, J. Liu, and W.-L. Zhao, Observing the exponential growth of the eigenmodes in the absence of coalescence for a non-Hermitian circuit with an unavoidable inductor dissipation, *Phys. Rev. A* **112**, 052211 (2025).
- [85] T. Li and H. Hu, Floquet non-Abelian topological insulator and multifold bulk-edge correspondence, *Nat. Commun.* **14**, 6418 (2023).
- [86] R.-J. Slager, A. Bouhon, and F. N. Ünal, Non-Abelian Floquet braiding and anomalous Dirac string phase in periodically driven systems, *Nat. Commun.* **15**, 1144 (2024).
- [87] J. Pan and L. Zhou, Floquet Non-Abelian Topological Charges and Edge States, *Chin. Phys. Lett.* **42**, 090706 (2025).
- [88] Z. Gong, Y. Ashida, K. Kawabata, K. Takasan, S. Higashikawa, and M. Ueda, Topological Phases of Non-Hermitian Systems, *Phys. Rev. X* **8**, 031079 (2018).
- [89] H.-Y. Wang, F. Song, and Z. Wang, Amoeba Formulation of Non-Bloch Band Theory in Arbitrary Dimensions, *Phys. Rev. X* **14**, 021011 (2024).
- [90] E. J. Bergholtz, J. C. Budich, and F. K. Kunst, Exceptional topology of non-Hermitian systems, *Rev. Mod. Phys.* **93**, 015005 (2021).

TABLE I. Summary of the topology and edge modes surviving criticality in PQNHSSH  $\alpha$ -chain along phase boundaries in Fig. 2. Here,  $J_{\alpha'} \equiv \sqrt{J_{\alpha'}^L J_{\alpha'}^R}$  and  $J_{\alpha'}^L J_{\alpha'}^R = J^2 - \gamma^2$ . The two Floquet bands are touched at gapless quasienergy.

Critical line	Condition	Gapless quasienergy	Topological invariants $(w_0, w_\pi)$	Number of edge modes $(N_0, N_\pi)$
Solid	$ \tan(J_{\alpha'}/2)  =  \tan(J_\alpha/2) $ $ \tan(J_{\alpha'}/2) \tan(J_\alpha/2)  < 1$	$E = 0$	$(\alpha, 0)$	$(2\alpha, 0)$
Dashed	$ \tan(J_{\alpha'}/2)  =  \tan(J_\alpha/2) $ $ \tan(J_{\alpha'}/2) \tan(J_\alpha/2)  > 1$	$E = 0$	$(\alpha, \alpha' - \alpha)$	$(2\alpha, 2\alpha' - 2\alpha)$
Dotted	$ \tan(J_{\alpha'}/2) \tan(J_\alpha/2)  = 1$ $ \tan(J_{\alpha'}/2)  <  \tan(J_\alpha/2) $	$E = \pm\pi$	$(\alpha, 0)$	$(2\alpha, 0)$
Dash-dotted	$ \tan(J_{\alpha'}/2) \tan(J_\alpha/2)  = 1$ $ \tan(J_{\alpha'}/2)  >  \tan(J_\alpha/2) $	$E = \pm\pi$	$(\alpha', 0)$	$(2\alpha', 0)$
Multicritical	$ \tan(J_{\alpha'}/2)  =  \tan(J_\alpha/2) $ $ \tan(J_{\alpha'}/2) \tan(J_\alpha/2)  = 1$	$E = 0, \pm\pi$	$(\alpha, 0)$	$(2\alpha, 0)$

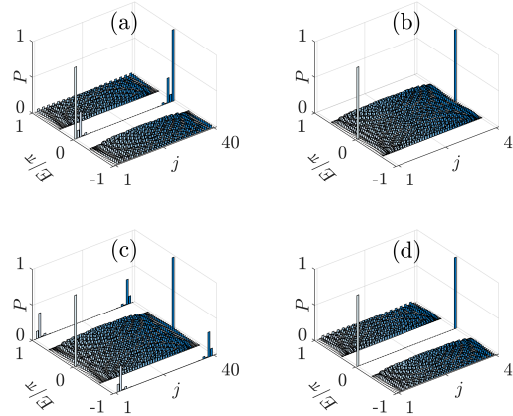


FIG. 6. Quasienergy-resolved probability distributions  $P$  of bulk and edge modes in the PQNHSSH  $\alpha$ -chain under OBC with 20 unit cells.  $j$  is the lattice index. Other parameters of (a)–(d) are the same as those of (a), (b), (d) and (e) in Fig. 3.

## END MATTER

For the PQNHSSH  $\alpha$ -chain with  $(\alpha, \alpha') = (1, 2)$ , we find two possible Floquet eigenstates at quasienergy 0 and one at quasienergy  $\pi$  when considering a half-infinite chain with the OBC taken at its left edge. The wavefunctions of these eigenmodes are given by (see Sec. II of the SM for details)

$$|\varphi_{0,1}\rangle = \hat{a}_1^\dagger |\emptyset\rangle, \quad (6)$$

$$|\varphi_{0,2}\rangle = \sum_{n=1}^{\infty} \left[ -\frac{\tan(J_1/2)}{\tan(J_2/2)} \right]^n \left[ \cos(J_1/2) \hat{a}_{n+1}^\dagger - i \sin(J_1/2) \hat{b}_n^\dagger \right] |\emptyset\rangle, \quad (7)$$

$$|\varphi_\pi\rangle = \sum_{n=1}^{\infty} \left[ \frac{1}{\tan(J_1/2) \tan(J_2/2)} \right]^n \left[ \sin(J_1/2) \hat{a}_{n+1}^\dagger + i \cos(J_1/2) \hat{b}_n^\dagger \right] |\emptyset\rangle. \quad (8)$$

where  $J_2 \equiv \sqrt{J^2 - \gamma^2}$ . Each of the states, when exists, has a degenerate partner in thermodynamic limit due to the sublattice symmetry. We see that the state  $|\varphi_{0,1}\rangle$  represents an edge 0 mode throughout the phase diagram, ensuring the nontrivial topology of all critical lines. The mode  $|\varphi_{0,2}\rangle$  is localized, delocalized and eliminated when  $|\tan(J_1/2)/\tan(J_2/2)| < 1$ ,  $= 1$  and  $> 1$ , respectively. It thus depicts an edge 0 mode when  $|\tan(J_2/2)| > |\tan(J_1/2)|$ , which survives along the critical lines where  $|\tan(J_1/2) \tan(J_2/2)| = 1$  and the bulk gap closes at quasienergy  $\pi$ . The mode  $|\varphi_\pi\rangle$  is localized, delocalized and eliminated when  $|\tan(J_1/2) \tan(J_2/2)| > 1$ ,  $= 1$  and  $< 1$ , respectively. It then describes an edge  $\pi$  mode when  $|\tan(J_1/2) \tan(J_2/2)| > 1$ , which survives along the critical lines where  $|\tan(J_1/2)| = |\tan(J_2/2)|$  and the bulk gap closes at quasienergy 0. These results, as deduced from Eqs. (6)–(8), are all consistent with the predictions summarized in Table I.